Journal of Proteomics 181 (2018) 213–224

Contents lists available at ScienceDirect

Journal of Proteomics

journal homepage: www.elsevier.com/locate/jprot

Fasting and refeeding induces changes in the mouse hepatic lipid droplet proteome

David A. Kramer[a,1], Ariel D. Quiroga[b,c,1], Jihong Lian[d,e], Richard P. Fahlman[a,f,*], Richard Lehner[d,e,g,**]

[a] Department of Biochemistry, University of Alberta, Edmonton, AB, Canada
[b] Instituto de Fisiología Experimental (IFISE), Facultad de Ciencias Bioquímicas y Farmacéuticas, CONICET, UNR, Rosario, Argentina
[c] Área Morfología, Facultad de Ciencias Bioquímicas y Farmacéuticas, UNR, Rosario, Argentina
[d] Department of Pediatrics, University of Alberta, Edmonton, AB, Canada
[e] Group on Molecular and Cell Biology of Lipids, University of Alberta, Edmonton, AB, Canada
[f] Department of Oncology, University of Alberta, Edmonton, AB, Canada
[g] Department of Cell Biology, University of Alberta, Edmonton, AB, Canada

ARTICLE INFO

Keywords:
Lipid droplet
Liver
Organelle
Proteome
Label free proteomics

ABSTRACT

During fasting, the liver increases lipid storage as a mean to reserve and provide energy for vital cellular functions. After re-feeding, hepatocytes rapidly decrease the amount of triacylglycerol that is stored in lipid droplets (LDs), visible as the size of hepatic LDs significantly decreases after re-feeding. Little is known about the changes in the liver LD proteome that occur during the fasting/re-feeding transition. This study aimed to investigate the hepatic LD proteome in fasted and re-fed conditions in the mouse. Using label-free LC-MS/MS analysis the relative abundance of 817 proteins was determined in highly purified LDs. Comparative analysis for differential protein abundance with respect to feeding states revealed 130 with higher abundance in LDs from fasted mice and 31 in LDs from re-fed mice. Among proteins observed to have higher abundance on LDs in the fasted state we found perilipin-5, and several mitochondrial and peroxisomal marker proteins, supporting the role of LDs in the provision of substrates for fatty acid oxidation. Proteins of higher abundance upon re-feeding included several peroxisomal and mitochondrial marker proteins and expand our understanding of the dynamic nature of the hepatic LD proteome according to the energetic requirements of the cell.

Biological Significance: Proteomic investigations have been revealing the complexities and dynamics of cellular LDs from a variety of cell types. As these sub-cellular structures are truly dynamic in nature, our investigations reveal that simply the feeding state of an animal leads to significant changes to the protein composition of LDs and suggest a variety of dynamic interactions with other cellular organelles, such as the mitochondria and peroxisomes. As such, the experimental design for investigations of this cellular structure must consider this dynamic baseline. Lastly our analysis on global protein abundance has revealed the unforeseen high abundance of murine major urinary proteins associated with hepatic lipid droplets, which warrants further investigations.

1. Introduction

Lipid Droplets (LDs) are cytoplasmic organelles ubiquitous to all cells and species [for reviews see Refs. [1, 2]]. LDs have been proposed to play important roles in many cellular processes including lipid metabolism, signal transduction, protein storage and lipid trafficking [3]. Hepatic LDs contain mainly triacylglycerol (TG), with some cholesteryl ester and retinyl ester as a neutral lipid core and are central to abnormal lipid accumulation during hepatic steatosis [4]. This core is surrounded by a monolayer of amphipathic lipids (phospholipids and free cholesterol) and LD-associated proteins of the PAT (Perilipin-1, ADRP/Perilipin-2, TIP47/Perilipin-3) family [for reviews see [1–3,5]]. In addition, proteomic studies have shown that a variety of proteins, other than PAT proteins, interact with LDs (either embedded or associated), thus enabling the multiple functions of this organelle [6–8]. Moreover, based on the characteristics of the identified LD proteins, LDs

Abbreviations: ER, endoplasmic reticulum; LDs, lipid droplets; TG, triacylglycerol

* Correspondence to: Richard P. Fahlman, Department of Biochemistry, University of Alberta, Edmonton, AB, Canada.
** Correspondence to: Richaerd Lehner, Department of Pediatrics, University of Alberta, Edmonton, AB, Canada.
E-mail addresses: rfahlman@ualberta.ca (R.P. Fahlman), rlehner@ualberta.ca (R. Lehner).

[1] Equal contribution.

https://doi.org/10.1016/j.jprot.2018.04.024
Received 22 December 2017; Received in revised form 10 April 2018; Accepted 14 April 2018
Available online 23 April 2018

are now known to interact with various other cellular compartments including the endoplasmic reticulum (ER), mitochondria, peroxisomes, endosomes and the cytoskeleton [reviewed in [9,10]].

During fasting, the liver enters a state of physiological steatosis, increasing lipid storage in LDs as a mean to reserve and provide energy for vital cellular functions. The source of fatty acids for hepatic TG synthesis are non-esterified fatty acids derived from hydrolysis of TG stored in the adipose tissue, dietary fatty acids from intestinal chylomicron remnants, and fatty acids newly synthesized through de novo lipogenesis. Because fatty acids exert deleterious effects on cellular functions when in their free form (biological detergents at neutral pH), excess fatty acids are esterified into TG. In the liver, TG can be either stored in LDs or secreted in TG-rich apoB-containing lipoproteins into the bloodstream. TG can also be hydrolyzed and fatty acids directed toward mitochondrial β-oxidation. As determined empirically by others [11], after re-feeding, hepatocytes rapidly decrease the number and size of LDs; however, little is known about the physiology of this process and the changes in the proteome during the fasting/re-feeding transition that allow for this process to occur.

This study aimed to investigate the hepatic LD proteome in fasted and re-fed conditions in the mouse using gel-LC-MS/MS analysis. Our findings reveal unexpected changes in the LD proteome in fasting versus re-fed livers.

2. Experimental procedures

2.1. Animals and feeding conditions

We utilized 4-month-old male C57BL/6 mice, with each individual LD sample prep comprised of the livers of 3 animals. Mice were fed ad libitum a chow diet (LabDiet, PICO Laboratory Rodent Diet 20, 23.9% protein, 5% fat, 48.7% carbohydrates). Mice were randomly split into two groups: fasted (24 h fast) and re-fed (24 h fast followed by 6 h re-feeding). All animal procedures were approved by the University of Alberta's Animal Care and Use Committee and were in accordance with guidelines of the Canadian Council on Animal Care. Mice, housed three to five per cage, were exposed to a 12 h light/dark cycle beginning with light at 8:00 a.m.

2.2. Lipid droplet fractionation

At the end of each feeding period mice were sacrificed by cardiac puncture, livers were harvested, rinsed in ice-cold PBS and immediately subjected to homogenization with a motor-driven potter in a hypotonic lysis medium (HLM, 20 mM Tris·Cl, pH 7.4, 1 mM EDTA). All solutions included protease inhibitors (EDTA-free Complete protease inhibitors, Roche Diagnostics) and phosphatases inhibitors (PhosSTOP, Roche Diagnostics). LDs were isolated according to Brasaemle and Wolins, 2006 [12], with some modifications [13]. Homogenates were spun at 500 ×*g* for 10 min. Supernatants were then spun at 15,000 ×*g* for 10 min to remove mitochondria and to allow fat cake separation. Fat cakes were transferred into new tubes and washed twice at same speed and length of centrifugation. Fat cakes were then diluted 1/3 in 60% sucrose in order to obtain 20% density adjusted suspensions. These were layered at the bottom of ultracentrifuge tubes and overlaid with double the volume HLM-5% sucrose, followed by careful overlay with same volume of HLM. Samples were centrifuged at 28,000 ×*g* for 30 min and fat cakes were carefully recovered and analyzed.

2.3. Solubilization of lipid droplet–associated proteins for western blot and LC-MS/MS analysis

To solubilize LD-associated proteins for subsequent Western blot and LC-MS/MS procedures, fresh LD fractions prepared from fasted (n = 3) and refed (n = 3) mice were mixed with 10% sodium dodecyl sulfate (SDS) (1:1, v/v) and incubated for 1 h at 37 °C in a sonicating water bath with constant agitation. Then, samples were microcentrifuged 10 min at maximum speed, at room temperature and the infranatants containing the solubilized proteins were collected from beneath the floating lipid layer. Equivalent volumes of 2× SDS sample buffer were added to the samples, which were then boiled for 10 min prior to loading equivalent amounts of total protein onto a discontinuous SDS-PAGE gel.

2.4. Sample preparation for mass spectrometry

SDS-PAGE gels were visualized with R-250 coomassie blue protein stain (SigmaAldrich). Once visualized, protein bands were excised in segments, as outlined in Supp. Fig. 1. Each gel section was individually treated to in-gel tryptic digestion as previously described [14].

2.4.1. LC-MS/MS of lipid droplet-associated proteins

Fractions containing tryptic peptides dissolved in aqueous 5% v/v ACN and 1% v/v formic acid were resolved and ionized by using nanoflow HPLC (Easy-nLC II, Thermo Scientific) coupled to a LTQ XL-Orbitrap hybrid mass spectrometer (Thermo Scientific). Nanoflow chromatography and electrospray ionization were accomplished with a PicoFrit fused silica capillary column (ProteoPepII, C18) with 100 μm inner diameter (300 Å, 5 μm, New Objective). Peptide mixtures were resolved at 500 nL/min using 60 min linear ACN gradients from 0 to 45% *v*/v aqueous ACN in 0.2% v/v formic acid. The mass spectrometer was operated in data-dependent acquisition mode, recording high-accuracy and high-resolution survey Orbitrap spectra using external mass calibration, with a resolution of 60,000 and *m/z* range of 400–2000. The ten most intense multiply charged ions were sequentially fragmented by using collision induced dissociation, and spectra of their fragments were recorded in the linear ion trap; after two fragmentations, all precursors selected for dissociation were dynamically excluded for 60 s. Raw data was processed using Proteome Discoverer 1.4.1.14 (Thermo Scientific) and a reviewed, non-redundant *Mus musculus* complete proteome FASTA index (UniprotKB – retrieved October 2015) protein database was searched using SEQUEST (Thermo Scientific). Search parameters included a precursor mass tolerance of 10 ppm and a fragment mass tolerance of 0.8 Da. Peptides were searched with static modifications as we have previously described [15]. The 'Precursor Ion Area Detector' node was implemented in the data processing workflow to determine relative extracted ion chromatograms (EICs) for each protein identified. Processed data was then filtered using a minimum of 2 medium-confidence (FDR < 0.05) peptides per protein, the data from this analysis is listed in Supp. Table 1. False discovery rate thresholds for peptide confidence were as follows; Fasted-1: Strict FDR = 0.0097; Fasted-2: Strict FDR = 0.0097; Fasted-3: Strict FDR = 0.0097; *Re*-Fed-1: Strict FDR = 0.0097; Re-Fed-2: Strict FDR = 0.0097; Re-Fed-3: Strict FDR = 0.0092. Protein lists from were then exported and compared using Microsoft Excel.

The mass spectrometry proteomics data have been deposited to the ProteomeXchange Consortium via the PRIDE [16] partner repository with the dataset identifier PXD005977.

2.4.2. Mass spectrometry data analysis and network analysis

To simplify data analysis, notable contaminants (keratins) were removed from the data set. Likewise, proteins with an observed EIC in ≤1 sample across all n = 6 samples were removed. The remaining data was corrected by normalizing identified proteins' EICs to the observed perilipin-2 EIC in a sample-specific manner. The corrected protein abundances (EIC-*corr*) for each protein were averaged among samples within their respective experimental condition (fasted versus re-fed). To determine relative changes in average protein abundance between experimental conditions, $\log_2$(EIC-$corr_{fasted}$/EIC-$corr_{refed}$) ratios were generated. To determine the significance of the changes observed, a two-tailed heteroscedastic Student's *t*-test was applied to each protein's EIC-*corr* array between experimental conditions; once grouped, proteins

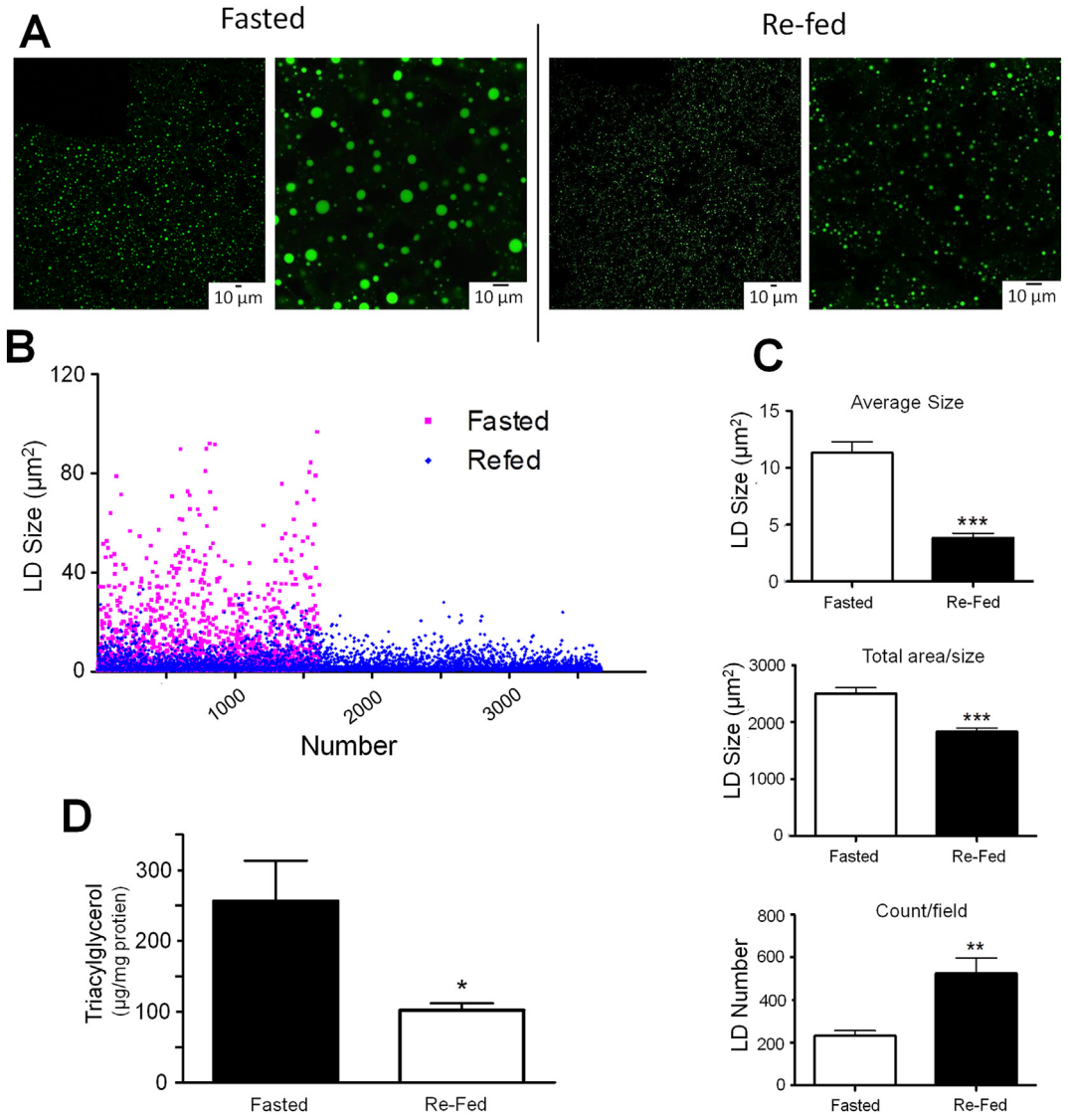

Fig. 1. Liver LD morphology during fasting and re-feeding. (A) Representative images of hepatic LDs. Bar = 10 µm. (B) Distribution of hepatic LDs from fasted and re-fed mice. Seven images were taken from four sections of each condition (100× objective at a zoom-factor of 2), sizes and numbers of LDs were analyzed and pooled. Each data point represents an individual LD. (C) Average area of an individual LD, total area of LDs per image field, and number of LDs per image field. (D) Liver triacylglycerol concentration in fasted and re-fed states. *P < 0.05, **P < 0.01, ***P < 0.001.

unique and significantly up-regulated ($p < 0.05$ and/or ≥ 6-fold change in abundance) in each condition were searched using the STRING 10.0 web-utility and enriched for KEGG pathways and the Gene Ontologies: Molecular Function, Biological Processes, and Cellular Components. Output lists were exported to Microsoft Excel and only ontologies and pathways with an FDR ≤ 0.05 were utilized.

While the utilization of label-free proteomic quantification is most effective when comparing the abundance of individual proteins between samples, as described above, the comparison of proteins' absolute abundances within a sample can provide valuable information with respect to total protein composition. Bias exists when comparing peptides from different proteins within a sample due to the different ionization efficiencies of the various tryptic peptides, in conjunction with a large dynamic range of protein abundance; while this hinders absolute quantitative comparisons within a sample, it has been observed that label-free proteomic quantification methods do correlate with global protein abundance [17]. As such, in addition to our comparative analysis using relative ion intensities, we performed compositional analysis of LD protein abundance across all datasets using normalized peptide spectral matches (PSMs), relative to Plin2.

2.5. Western blotting and immunostaining of membranes

Proteins were resolved by SDS-PAGE (10%) based either on the same triacylglycerol or protein concentrations and were transferred onto PVDF membranes. Specific primary antibodies were incubated with the membranes overnight after blocking the membrane with 5% *w/v* skimmed milk for 1 h at room temperature. The following primary antibodies, with their working dilutions from the stock solutions obtained from the supplier in 3% w/v BSA in TBST, were used: acyl-CoA synthetase/ligase 1 (Acsl1) (1:1000, Cell Signaling, #4047), perilipin 2 (Plin2) (1:1000, Abcam #108323), perilipin 5 (Plin5) (1:2000, Progen #GP31), calnexin (Cnx) (1:1000, Enzo Life Sciences #SPA-865), β-actin (1:1000, Cell Signaling, #4967), carboxylesterase 1d (Ces1d, also called Ces3 or TGH) that also reacts with carboxylesterase 1 g (Ces1g, also called Ces1 or Es-x) (1:30000, generated in-house [18]), major urinary protein 1 (MUP1*) (1:300, Santa Cruz Biotechnology #SC-66976), glyercaldehyde 3-phosphate dehydrogenase (GAPDH) (1:5000, Abcam #ab8245), and phosphatidylethanolamine-*N*-methyltransferase (Pemt) (1:1000, generous gift from Dr. Dennis Vance [19]). The following secondary antibodies, diluted 1:5000 in 5% w/v skimmed milk in TBST,

were incubated for 1 h at room temperature: HRP-labelled donkey anti-guinea pig IgG (Fitzgerald #43R-ID039hrp) and HRP-labelled goat anti-rabbit IgG (Invitrogen #31460). Immunoreactive proteins were detected by enhanced chemi-luminescence (GE Healthcare, UK) using HRP-labelled secondary antibodies.

2.6. Histological analysis

Livers collected from mice from both fasted and re-fed conditions were embedded in OCT and frozen for further histological analysis. Frozen liver sections were stained with 2 μg/ml BODIPY 493/503 (Invitrogen, USA) in PBS for 1 h at room temperature to visualize LDs. Images were collected with a laser scanning confocal microscope (Leica TCS SP5, software version *Leica LAS AF 2.6.0,* Leica, Germany). Quantification of LD number and size was done with ImageJ software (NIH, USA).

2.7. RNA isolation and real-time qPCR analysis

Liver total RNA was isolated using Trizol reagent (Invitrogen, USA). First-strand cDNA was synthesized from 2 μg total RNA using Superscript III reverse transcriptase (Invitrogen) primed by Oligo $(dT)_{12–18}$ (Invitrogen) and random primers (Invitrogen). Real-time qPCR was performed with Power SYBR® Green PCR Master Mix kit (Life Technologies, UK) using the StepOnePlus-Real time PCR System (Applied Biosystems, Canada). Real-time qPCR primers, whose sequences are outlined below, were synthesized by Integrated DNA Technologies (USA). Data were analyzed with the StepOne software (Applied Biosystems). A standard curve was used to calculate mRNA abundance relative to that of a control gene, cyclophilin.

Primer sequences: Cyclophilin (F: 5′-TCCAAAGACAGCAGAAAACT TTCG-3′, R: 5′-TCTTCTTGCTGGTCTTGCCATTCC-3′), Plin2 (F: 5′-CAC TCCACTGTCCACCTGATT-3′, R: 5′-TCCTGAGCACCCTGAATTTT-3′), Plin3 (F: 5′-GGAGGAACCTGTTGTGCAG-3′, R: 5′-ACCATCCCATACGT GGAACT-3′), Plin5 (F: 5′-TGTGTGTAGTGTGACTACCTGTGC-3′, R: 5′-GGCAAGATCATTCACTGTGG-3′), and ACSL1 (F: 5′-CCACCATCTTC CCTGTGG-3′, R: 5′-GGAAGTGTTTGCTTGTCCAAA-3′).

3. Results

3.1. Liver morphology during fasted and Re-fed states

The liver accumulates TG after 24 h fast due to the high fatty acid flux from the adipose tissue leading to significant increase in individual LD size and total area (Fig. 1A–C), reflecting what has been reported previously [11]. Consequential of re-feeding the animals for 6 h after a 24 h fast, the average area of an individual LD decreased by 66% while the total LDs area decreased by 27% (Fig. 1A–C). Concurrently, the number of LDs increased by 126% after re-feeding (Fig. 1C), possibly due to the increased nascent LDs generated from induced de novo lipogenesis. Accordingly, hepatic TG levels were 1.5-fold lower after re-feeding the animals for 6 h compared with fasted mice (Fig. 1D).

3.2. Preparation and purity of LDs

Livers from fasted and re-fed animals were manually dissected, and LDs were released from the tissue and subsequently purified by sucrose density centrifugation. LD-associated proteins were delipidated, resolved by SDS-PAGE, where gel sections were individually treated to in gel tryptic digestion and analyzed by LC-MS/MS as outlined in Supp. Fig. 1. The purity of LDs was evaluated by immunoblot analysis. As shown in Fig. 2, LD-associated protein perilipin-2 (Plin2) was found in LD fractions from all samples. Calnexin (Cnx), a resident ER protein, was also present in all the studied samples. One particular interest is the partition pattern of ER carboxylesterases. Carboxylesterases Ces1d [also called triacylglycerol hydrolase, previously annotated as Ces3] and

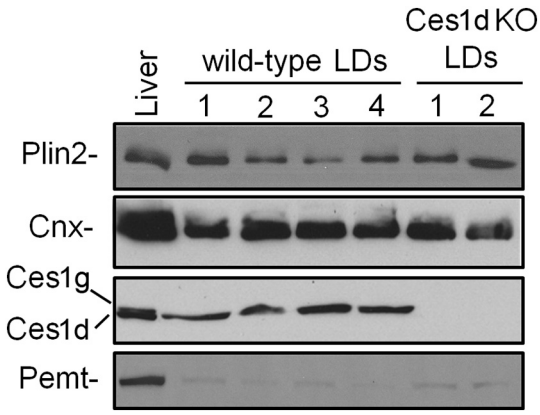

Fig. 2. Analysis of protein markers in purified LDs. Purified LDs from livers of four wild type mice or 2 Ces1d knockout mice were analyzed by Western Blotting for the indicated proteins. Liver homogenate from wild type mice (Liver) was used as a control.

Ces1g [also called esterase-x, previously annotated as Ces1] are related carboxylesterases present in the lumen of the ER. Interestingly, Western blot analysis revealed Ces1d (lower band) visibly partitioned to LDs, while Ces1g (upper band) was absent (Fig. 2). To additionally verify the identity of the lower band being Ces1d, LDs isolated from Ces1d knockout mice [20] were included for comparison (Fig. 2). An ER resident polytopic membrane protein phosphatidylethanolamine *N*-methyltransferase (Pemt) was essentially absent from isolated LDs (Fig. 2).

3.3. LD-associated proteins in the liver

The lipid droplets purified from the livers of nine fasted mice and nine ref-fed mice were then analyzed by gel-LC-MS/MS and the data was refined as described in the Materials and Methods. From this analysis (Supp. Table 2), 810 proteins were identified in the LDs isolated from the fasting mice and 784 were identified in the LDs from the re-fed mice (Fig. 3A). Of these, 7 were unique to the re-fed LDs and 33 unique to the fasted LDs. In comparison to previous investigations of the liver LD proteome have identified associated proteins ranging from 1520 [21] to only 134 [22].

To further investigate the quality of the data set, all the proteins observed were queried by gene ontology (GO) analysis using the PANTHER database [23]. For this analysis, an enrichment is determined by comparing the ontological frequency of identified proteins to that of the entire mouse proteome. GO analysis of all the proteins observed in the fasted and fed states revealed an enrichment for proteins that have been annotated to various organelles such as the ER, mitochondria, nuclear envelope, and peroxisomes, while being depleted for nuclear and plasma membrane proteins (Fig. 3B). While several proteins observed may reflect molecular contaminants resulting from purification procedure limitations, many of the enrichments observed in our data reflect the current perception of the dynamic nature of LDs; there is an increasing understanding of LD association to the various organelles within a cell [10]. Further GO analysis for biological functions of the identified proteins using Cytoscape v3.5.1 [24] with the ClueGO plugin [25] reflects the diversity observed with respect to the cellular localization of the annotated proteins. As summarized in Supp. Fig. 2, in addition to the major expected networks of metabolism and macromolecular complex assembly, significant numbers of proteins have been annotated for a variety of RNA metabolic processes such as heterocycle and aromatic biosynthesis, nucleoside phosphate metabolism and gene expression.

Quantitative analysis of the EIC intensities of the proteins identified in both the fasted and re-fed LD datasets revealed changes in proteins abundance upon re-feeding, the resulting data of which is summarized

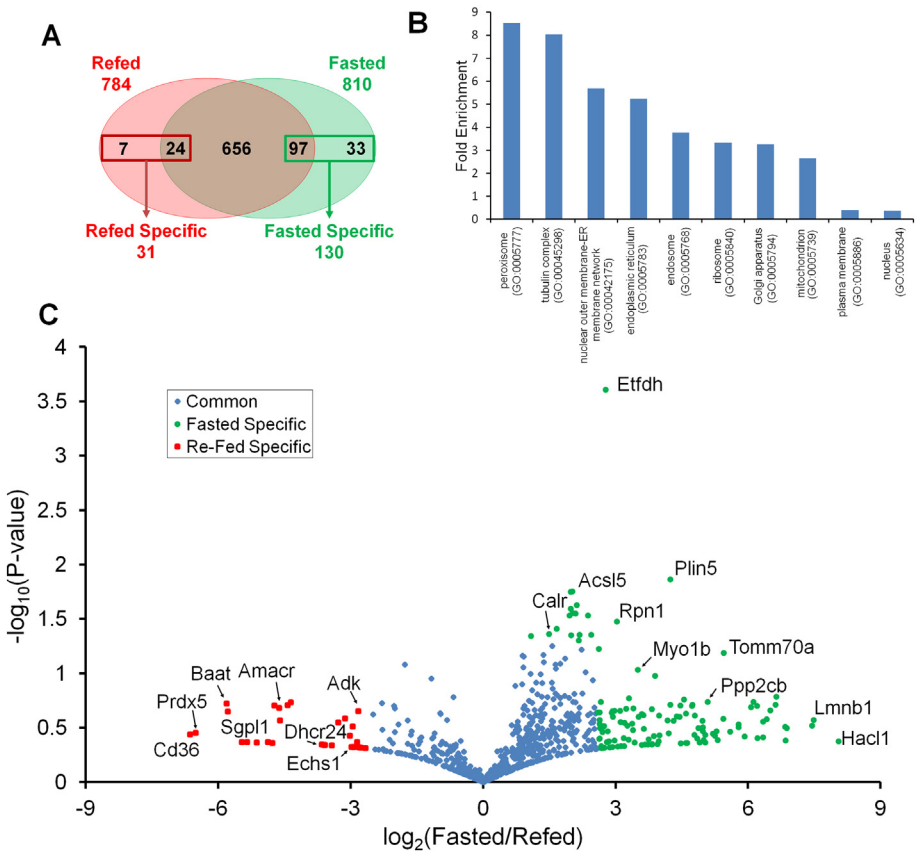

Fig. 3. Distribution of hepatic LD proteins during fasting and re-feeding. (A) Venn diagram showing the cross-correlation of identified hepatic LD-associated proteins in fasted (green) and re-fed (red) mice. Numbers enclosed in boxes represent proteins unique (not in central overlap) or determined to be more abundant, by comparison of the ion intensities of the peptides derived from the proteins (within central overlap), to a specific feeding condition. (B) GO analysis enrichment for cell localization for all proteins identified on LDs in both the fasted and re-fed datasets. (C) Volcano plot of proteins identified among both energetic states. The x-axis represents the fold-change in average protein abundance observed between fasted and re-feeding conditions as the function $\log_2$ of the corrected extracted ion chromatograms. The y-axis plots the statistical significance of the fold-difference observed between the states as the function -$\log_{10}$(*P*-Value). (For interpretation of the references to colour in this figure legend, the reader is referred to the web version of this article.)

in the volcano plot depicted in Fig. 3C. To facilitate the depiction of proteins uniquely observed in a single experimental condition on the log scale plot and provide an estimate of their minimal fold change, proteins with an average EIC = 0 for an experimental condition were deemed to be missing not at random (MNAR) and assigned values of the global minimum observed within their dataset. The abundance and distribution of all identified LD-associated proteins are listed in Suppl. Table 2 and those observed to change in abundance following data refinement are listed in Supp. Table 3.

3.4. Pathway analysis of dynamic LD-associated proteins

Utilizing STRING 10.0, KEGG pathway analyses [26] of the 130 LD proteins determined to be significantly more abundant in the fasted experimental condition revealed thirteen distinct pathways (excluding KEGG ID: 1100 – “Metabolic Pathways”) to be up-regulated; these include: ER protein processing, peroxisomal proteins, propanoate metabolism, valine/leucine/isoleucine degradation, fatty acid metabolism, TCA cycle, carbon metabolism, peroxisome proliferator-activated receptor (PPAR) signaling pathway, pyruvate metabolism, arginine and proline metabolism, microbial metabolism in diverse environments, antigen processing and metabolism, and fatty acid degradation. The complete list of these pathways and the proteins identified within these pathways are listed in Table 1. A complete list of all proteins observed to change in abundance are in Supp. Table 3. Interestingly, significantly less pathways were identified using this technique for the 31 proteins determined to be significantly more abundant during the re-fed state; only two pathways were observed (excluding KEGG ID: 1100 – “Metabolic Pathways”); peroxisomal proteins and primary bile acid biosynthesis (Table 2). While several of the pathways in both feeding states are populated by individual proteins, we believe this provides additional evidence of the diverse functions these organelles are capable of within the cell.

As pathway analysis revealed an enrichment of different peroxisome-associated proteins in both fasted and re-fed datasets (Tables 1 & 2), in addition to peroxisomal proteins exhibiting the highest fold-enrichment in the entire dataset (Fig. 3B), we further evaluated the data for these protein changes. The quantified data from the replicate analysis of the 12 peroxisomal proteins identified by KEGG pathway analysis, in addition to the mitochondrial protein Acsl1 involved in fatty acid oxidation [27,28], as shown in Fig. 4, reveals the magnitude of change for each proteins' observed LD-association upon fasting and re-feeding. While Acsl1 exhibited an approximately 30% decrease in abundance upon re-feeding, this did not meet the cut-off criteria used to list proteins that significantly change. This apparent dichotomy of differential peroxisomal protein association is suggestive of unique roles for LD-peroxisome interactions during fasting or feeding. It must also be noted that while the analyses revealed an enrichment for peroxisomes based on these proteins' annotations, many are not exclusively peroxisomal and have additional sub-cellular localizations as well.

3.5. Global protein abundance

A challenge arising from proteomic investigations of sub-cellular purified components is determining what proteins are most relevant from those that are likely contaminants that undoubtedly remain even after purification. To address this, at least in part, we next investigated the proteomic data with respect to PSMs for all proteins across all data sets to obtain estimates of the most abundant proteins in the LD samples and less likely to be low abundance contaminants. The PSMs, normalized to protein length to compensate for the increased number of potential tryptic peptides generated from longer proteins, were compared to estimate which proteins are most abundant with respect to LD composition. From the raw data, Supp. Table 1, it is noted that Plin2 is the protein which makes up the largest fraction of the normalized PSMs, indicating this to be one of, if not the most abundant protein(s) in the

Table 1
KEGG pathway identifiers populated from the proteins enriched in LDs isolated from livers of fasted mice with an FDR < 0.01. Proteins identified in each pathway are listed.

Protein	Protein name	Metabolic pathways	Propanoate metabolism	Val, Leu and Ile degradation	Fatty acid metabolism	Citrate cycle (TCA cycle)	Carbon metabolism	Pyruvate metabolism	Arg and Pro metabolism	Microbial metabolism	Fatty acid degradation	Protein processing in ER	Peroxisome	PPAR signaling pathway	Antigen processing & presentation
Aass	Alpha-aminoadipic semialdehyde synthase	+													
Abat	4-aminobutyrate aminotransferase	+	+	+											
Acaca	Acetyl-CoA carboxylase 1	+	+		+			+							
Acadvl	Very long-chain specific acyl-CoA dehydrogenase	+			+						+				
Acsl5	Long-chain-fatty-acid–CoA ligase 5	+			+						+		+	+	
Aldh4a1	Delta-1-pyrroline-5-carboxylate dehydrogenase	+							+						
Apoa5	Apolipoprotein A-V													+	
Asah1	Acid ceramidase	+													
Cpt2	Carnitine O-palmitoyltransferase 2, mitochondrial				+						+			+	
Dlat	Dihydrolipoyllysine-residue acetyltransferase component of pyruvate dehydrogenase complex	+				+	+	+		+					
Dld	Dihydrolipoyl dehydrogenase	+		+		+	+	+		+					
Gpam	Glycerol-3-phosphate acyltransferase 1	+													
Hacl1	2-hydroxyacyl-CoA lyase 1												+		
Hibch	3-hydroxyisobutyryl-CoA hydrolase	+	+	+			+								
Hmgcl	Hydroxymethylglutaryl-CoA lyase	+		+									+		
Hsd17b2	Estradiol 17-beta-dehydrogenase 2	+													
Hspa5	78 kDa glucose-regulated protein											+	+		
Hspa8	Heat shock cognate 71 kDa protein											+	+		
Lman2	Vesicular integral-membrane protein VIP36											+			
Lpin1	Phosphatidate phosphatase LPIN1	+													
Man1a	Mannosyl-oligosaccharide 1,2-alpha-mannosidase IA	+										+			
Man2a1	Alpha-mannosidase 2	+													
Maoa	Amine oxidase [flavin-containing] A	+							+						
Ndufv2	NADH dehydrogenase [ubiquinone] flavoprotein 2	+													
Oat	Ornithine aminotransferase	+							+						
Pccb	Propionyl-CoA carboxylase beta chain	+	+	+			+			+					
Pcx	Pyruvate carboxylase, mitochondrial	+				+	+	+		+					
Pdia3	Protein disulfide-isomerase A3											+			+
Pdia4	Protein disulfide-isomerase A4											+			
Pex1	Peroxisomal membrane protein 11A												+		
Pex26	Peroxisome assembly protein 26												+		
Pex6	Peroxisome assembly factor 2												+		
Pigs	GPI transamidase component PIG-S	+													
Prodh	Proline dehydrogenase 1, mitochondrial	+							+						
Rpn1	Dolichyl-diphosphooligosaccharide–protein glycosyltransferase subunit 1	+										+			

(*continued on next page*)

Table 1 (*continued*)

Protein	Protein name	Metabolic pathways	Propanoate metabolism	Val, Leu and Ile degradation	Fatty acid metabolism	Citrate cycle (TCA cycle)	Carbon metabolism	Pyruvate metabolism	Arg and Pro metabolism	Microbial metabolism	Fatty acid degradation	Protein processing in ER	Peroxisome	PPAR signaling pathway	Antigen processing & presentation
Scp2	Non-specific lipid-transfer protein	+											+	+	
Sec63	Translocation protein SEC63 homolog											+			
Slc27a5	Bile acyl-CoA synthetase	+												+	
Suclg2	Succinyl-CoA ligase [GDP-forming] subunit beta	+	+			+	+			+					
Suox	Sulfite oxidase, mitochondrial									+					
Tecr	Very-long-chain enoyl-CoA reductase	+			+										
Txndc5	Thioredoxin domain-containing protein 5											+			
Uroc1	Urocanate hydratase	+													

purified LDs. The average normalized spectral counts across all datasets were then plotted in Fig. 5A in decreasing abundance relative to Plin2. The data reveals that only 57 proteins of the 817 identified make up 50% of the spectral counts in the experiment, which leads to an estimate that these proteins make up half of the protein abundance in the samples. Correspondingly, 314 and 633 proteins make up 90% and 99% of the spectral counts, respectively. The proteins that comprise 50% of the normalized spectral counts likely represent the most abundant proteins in the purified LDs and their identities are summarized in Fig. 5B.

The unexpected observation of the murine specific secreted major urinary proteins (Mups) populating the list of the 57 most abundant proteins, led to validation experiments of the association of these proteins in the hepatic LDs. Fractions from a sucrose gradient purification of LDs from the livers of fasted mice were resolved by SDS-PAGE and analyzed for total protein abundance by coomasie staining or immunoblotting for Plin2 or Mups (with an antibody specific for a range of Mup isoforms). As seen in Fig. 6, while much of the observed Mup isoforms we observed in the high density heavy membrane associated fraction of the gradient, a significant amount of the Mups are also observed in the low-density fraction containing the LDs.

With the spectral counts and ion intensities observed ranging over several orders of magnitude for the different proteins identified in purified LDs, we evaluated proteins that were determined to significantly change in abundance upon fasting and re-feeding; if only very low abundance proteins were observed to significantly change, it would suggest many of our observed differences may simply reflect statistical noise as a result of proteins being at or near the limit of their detection. The data representing LD-associated proteins that significantly change in abundance during fasting and feeding with respect to their relative ion intensities is overlaid on the plot in Fig. 5A. While there is a trend for proteins with low normalized PSMs to be more frequently observed significantly changing in abundance between feeding states using relative ion intensities, a large proportion of proteins with high normalized PSMs are also observed to significantly change based on their relative ion intensities (Fig. 5A). Acadvl, Cpt2, and Hspa5, identified to significantly change in abundance between feeding states, populate within the list of 57 proteins that make up 50% of the normalized spectral counts.

3.6. Immunoblot validation of LD associated proteins

To confirm the LD-association of some of the identified proteins, and their changes upon feeding state, we assessed their abundance in purified LDs and whole liver homogenates by immunoblotting. To control for equal loading of isolated LDs between feeding states, sample loading was normalized to the LDs' TG content. Whole liver homogenates were used to evaluate whether the changes observed in proteins associated with LDs is a result of changes in a protein's global cellular abundance, or a change in LD-association; whereas LD loading was normalized to TG content, whole liver homogenates were normalized to total protein.

Plin2 and Plin5 are well characterized LD-associated proteins that play an important role in the regulation of LD turnover by preventing adipose triglyceride lipase (ATGL) - catalyzed lipolysis [29,30]. Plin2/TG ratio did not significantly change in the purified LDs isolated from livers of fasted/refed mice (Fig. 7A). In agreement with our mass spectrometry data for Plin5 (Supp. Table 2), LDs purified from fasting livers contained higher Plin5 abundance compared to those from re-fed livers, consistent with diminished lipolysis and increased TG storage (Fig. 7A). Furthermore, both Plin2 and Plin5 exhibit larger increases in abundance, relative to total protein, in the whole liver homogenate upon fasting (Fig. 7B) consistent with increased expression of Plin2 and Plin5 mRNAs during fasting (Fig. 7C). In contrast, Acsl1 revealed an increase in abundance by mass spectrometry (Fig. 4) and Western blot analysis (Fig. 7A), but no changes were observed in the whole liver

Table 2
KEGG pathway identifiers populated from the proteins enriched in LDs isolated from livers of re-fed mice with an FDR < 0.01. Proteins identified in each pathway are listed.

Protein	Protein name	Metabolic pathways	Peroxisome	Val, Leu and Ile degradation
Idh2	Isocitrate dehydrogenase [NADP], mitochondrial	+	+	
Baat	Bile acid-CoA:amino acid N-acyltransferase	+	+	+
Ndufb9	NADH dehydrogenase [ubiquinone] 1 beta subcomplex subunit 9	+		
Adk	Adenosine kinase	+		
Atp6v1e1	V-type proton ATPase subunit E 1	+		
Amacr	Alpha-methylacyl-CoA racemase	+	+	+
Dhcr24	Delta(24)-sterol reductase	+		
Sgpl1	Sphingosine-1-phosphate lyase 1	+		
Echs1	Enoyl-CoA hydratase, mitochondrial	+		
Aox3	Aldehyde oxidase 3	+		
Ftcd	Formimidoyltransferase-cyclodeaminase	+		
Dhrs4	Dehydrogenase/reductase SDR family member 4	+	+	
Dpm1	Dolichol-phosphate mannosyltransferase subunit 1	+		
Prdx5	Peroxiredoxin-5, mitochondrial		+	

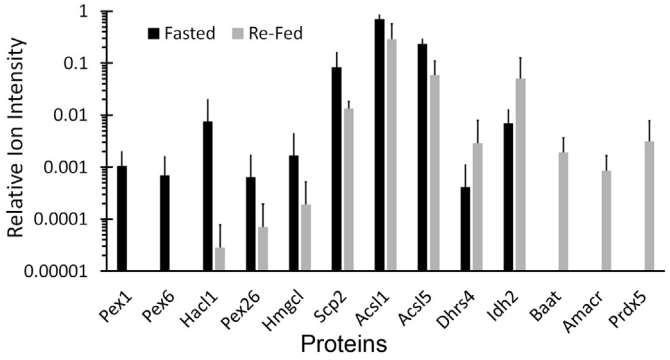

Fig. 4. Relative abundance of peroxisomal proteins associated with LDs isolated from the livers of mice after fasting (black) or re-feeding (light grey). Quantification is the average relative EICs, relative to Plin2, for each indicated protein from triplicate analysis.

homogenates (Fig. 7B), indicating a change in protein localization and not protein abundance in the cell. Interestingly, the expression of Acsl1 mRNA was decreased during refeeding (Fig. 7C) but this change was not translated into lower protein abundance suggesting a long half-life of the protein.

4. Discussion

4.1. Fasted and Re-fed liver LDs

The study presented here was designed to systematically identify the LD-associated proteome from the mouse liver during fasting and re-feeding. Two key issues when analyzing organelle proteomes are assessing the purity of the preparations, as well as how to correct datasets to reduce between-sample variability upon comparison. With respect to sample purity, we expectedly found the canonical LD-marker proteins in our LD preparations, including Plin2 and Plin3. Cnx, an ER-localized protein was present in all studied LD fractions (Fig. 2B); although the presence of this protein on the LD surface was previously reported [31], we analyzed the presence of another ER membrane protein Pemt in order to evaluate LD purity and possible ER contamination. Pemt was nearly completely absent from the isolated LD fractions (Fig. 2B), suggesting minimal contamination of our LD preparations with the ER. Luminal ER proteins (Bip, Pdi) have been previously found in LD preparations from various cells and tissues and a possible mechanism how such proteins could be targeted to LDs has been proposed [32,33].

Ces1d (Ces3/TGH) and Ces1g (Ces1/Es-x) are ER luminal resident lipid hydrolases containing the C-terminal ER-retrieval motif –HVEL [34–36]. Interestingly, we found by immunoblotting that Ces1d partitioned to the LDs, while its close family member Ces1g did not. The mechanism for such selectivity is unclear because both Ces1d and Ces1g were identified via LC-MS/MS on purified LDs from both fasted and refed conditions. Our studies showed that hepatocytes lacking Ces1d contain an increased number of smaller LDs compared to wild-type hepatocytes, suggesting that Ces1d plays a role in LD maturation [20]. The role of Ces1g in LD growth and maturation has not been evaluated, however; unlike Ces1d, lack of Ces1g leads to increased size and number of cytosolic LDs [37], showing functional differences between these two ER-localized carboxylesterases.

4.2. Global proteome analysis of liver LDs

Shotgun proteomics was used to characterize the murine hepatic LD proteome of fasted and re-fed mice. Our analysis identified a complete set of 817 proteins that are associated with purified with LD in both energetic states (Fig. 3A). GO analysis for cellular localization of the entire data set revealed a significant enrichment for proteins that have been annotated to a variety of sub-cellular localizations (Fig. 3B). The greatest enrichment observed was for peroxisomal proteins, in agreement with previous work demonstrating a close association between LDs and peroxisomes [38]. As both LDs and peroxisomes are key players in the lipid metabolic flux, their close interactions have been proposed to be key for bidirectional lipid trafficking [39]. As predicted, a depletion of nuclear and plasma membrane proteins was also observed. The enrichment of peroxisomal, ER, mitochondrial, and Golgi proteins was expected as there is a growing appreciation of the interaction and function of LDs with these organelles [9,10]. At first glance, other observed enrichments may appear to be contaminants, such as ribosomal proteins (Fig. 3B) and proteins involved in RNA metabolism (Supp. Fig. 2); however, these have been previously reported to be associated to the LD proteome [40,41] and have been verified by ultrastructural investigations [41]. The role of ribosomes in LDs is still unclear and remains an open question in LD biology [42]. However, early investigations with model organisms have suggested that LDs may also function as protein storage organelles [6]. Alternatively, the presence of highly abundant proteins in LDs may simply be an artifact of these proteins being trapped in LDs during their rapid formation and growth in the cell. Nonetheless, the agreement of our hepatic LD dataset with previous studies only strengthens these observations.

With ongoing proteomic studies of hepatic LDs, there is an increasing number of proteins identified as being LD-associated [21,22,43,44]. A challenge with these growing lists, as there is when performing proteomics on any organelle, is the analysis and follow-up of the data. As mass spectrometers become more sensitive, the limits of detection will continue to decrease to a point that far exceeds the organelle's biochemical purity. As a result, the instrument's high

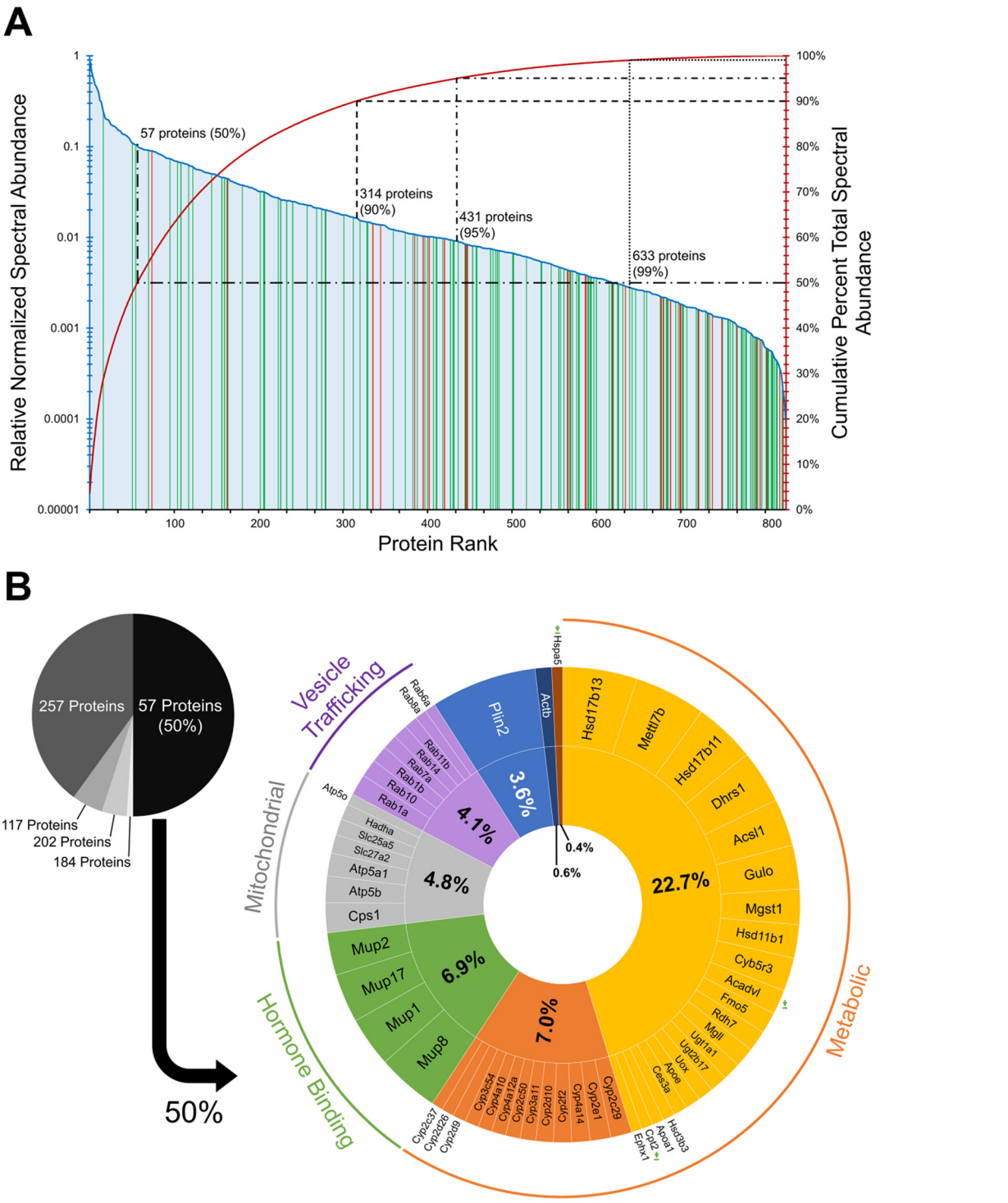

Fig. 5. Analysis of LD-associated proteins by spectral count abundance. A) All proteins detected are sorted by abundance, as determined by normalized spectral counting, relative to Plin2, the protein observed with highest number of normalized PSMs in the experiment. The number of proteins that make the total quantified signal, as determined by spectral counting, are indicated. Green horizontal bars indicate proteins with higher abundance in the hepatic LDs of fasted mice, while red bars indicate protein that are higher in abundance in re-fed mice. B) A graphic depiction and classification of the 57 proteins that make up 50% of the normalized spectral counts are shown. Green arrows indicate the proteins that are lower in abundance in the liver LDs of re-fed mice. (For interpretation of the references to colour in this figure legend, the reader is referred to the web version of this article.)

sensitivity can detect the low abundant contaminants that are undoubtedly present in the sample. To address this, we evaluated the data to identify the most abundant proteins in the LD proteome with respect to composition (Fig. 5). This perspective is reminiscent of early investigations of the LD proteome, where samples were resolved by SDS-PAGE and individual bands were excised and identified by mass spectrometry [45,46]. The identification of the most abundant proteins in the organelle proteome is predicted to validate well-known proteins already associated with the organelle or identify major components that have been previously overlooked. The 57 proteins that are estimated to make up 50% of the LD proteome (Fig. 5B) fall within both groups. In addition to the expected proteins such as the PAT domain family

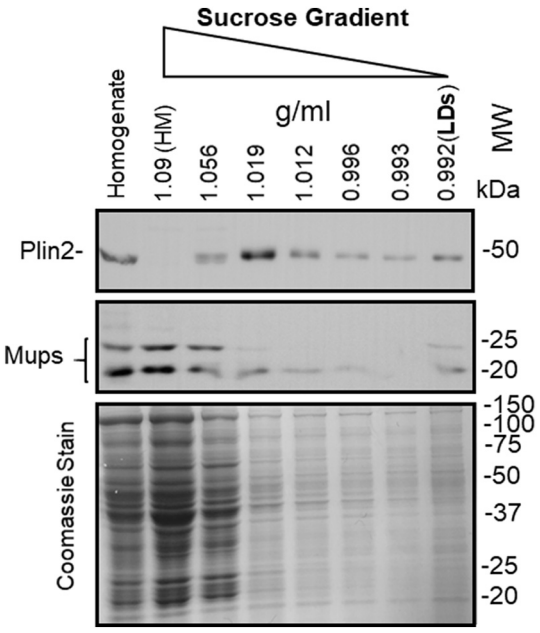

Fig. 6. Immunoblot analysis of sucrose gradient fractions reveal Mup association to LDs. Fractions from a sucrose gradient for the purification of LDs were resolved by SDS-PAGE and analyzed by: immunoblotting for Plin2 (upped panel), total protein by coomasie staining (lower panel) and, immublotting for Mups with an antibody targeting a range of Mup isoforms. The fractions containing the heavy membranes (HM) and lipid droplets (LDs) are indicated.

member, Plin2, and the most abundant group of proteins involved in metabolism (such as Acsl1), several other protein families are observed in high abundance. These include a series of Rab proteins which have been well described with respect to LD trafficking [45,47–54], in addition to a number of other enzymes also observed in high abundance from cell culture models such as a series of mitochondrial proteins [55]. Cytochrome P450 proteins have not historically been considered to be associated with LDs, nor were they significantly observed in LDs from hepatic cell lines [46]. However, they have been observed in multiple reports from liver-derived LDs and have been observed to increase in abundance in liver LDs during diet-induced hepatic steatosis [21,22,43].

The most unexpected protein family in our dataset observed in high compositional abundance were the murine specific Mups, a family of rodent specific proteins with roles in the transport and excretion of pheromones and other lipophilic molecules [56]. With the complexities of the metabolic reactions carried out by LD-associated enzymes, it is not surprising to observe an abundance of these lipophilic carrier proteins; the LD-association of Mups may potentially be where they are loaded with their cargo prior to secretion from the liver. Our observation of Mups being associated to LDs is not the first; supplemental data from other proteomic investigations of murine liver-derived LDs have also identified these proteins [21,22], but they were not discussed as they were not observed to change in abundance between experimental conditions. With our analysis, the Mups only stood out when we queried the data for the most compositionally-abundant proteins in the liver LD proteome. Being so highly abundant, the role of Mups' association with LDs warrants further investigation.

4.3. Dynamics of the LD Proteome Upon Feeding

As the focus of our investigations was on the dynamics of the hepatic LD proteome upon fasting and feeding, the quantitative analysis of the data was explored in greater detail. Analysis of our collected datasets (Supp. Table 2) revealed that 130 and 31 proteins were found to be more abundant in the fasted and re-fed LDs, respectively (Fig. 3A).

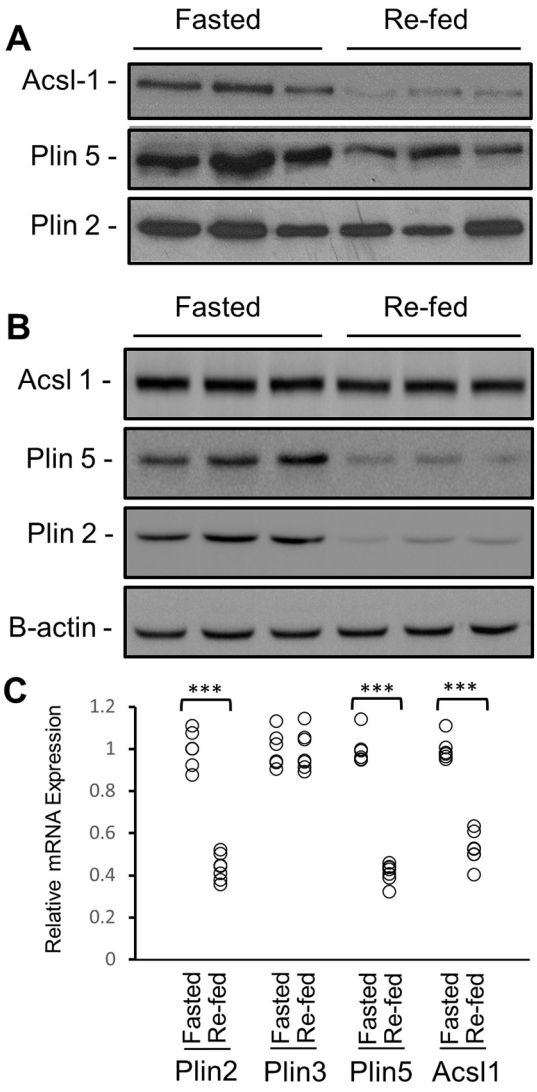

Fig. 7. Immunoblot analysis of representative LD-associated proteins from isolated LDs (A) and whole liver homogenates (B) from fasted and re-fed mice. Samples were analyzed on the basis of equal triacylglycerol content (A) or equal protein (10 μg) content (B) from fasted and re-fed mice. (C) RT-qPCR analysis of representative LD-associated proteins in livers from fasted and re-fed mice (N = 6–7). ***P < 0.001 vs. fasted group, the significance is based on two-tailed *t*-tests.

Of these changes, it is noteworthy that the catabolic proteins on LDs (Table 1) change between fasting and re-fed states, in agreement with the fact that lipid accumulation decreases after re-feeding (Fig. 1).

Previous LD proteomic screens with other cellular systems such as yeast [57], mammalian tissue culture [45,46] and germline cells [58] reveal hundreds of proteins with moderate overlap regarding protein composition. Comparing the LD proteomes originating from different tissues provides some insight into the core essential LD proteins and those which may be tissue specific. A comparison of our presented liver LD proteomes with that from the testes of mice [58] reveals an overlap of 159 proteins (Supp. Table 4), including the PAT domain family members Plin2 and Plin3, various lipid metabolizing enzymes, esterases, vesicular trafficking-associated proteins of the Rab- and chaperone-families. Recent reports on murine liver LDs, focusing on diet and disease models [22,43,44] such as hepatic steatosis [21] reveal even higher similarities to our dataset. In the context of these previous investigations, our presented work clearly highlights the dynamic changes undergone by the LD proteome simply upon feeding. As such, our work demonstrates how conditions must be carefully controlled

when investigating the LDs of various model systems. Additionally, it is interesting to note from these results how the LD proteome changes during different metabolic states to reflect functions other than fat storage. This provides a clearer picture of the dynamic nature of these organelles.

As the proteins that where observed in both higher and lower abundance upon re-feeding included proteins annotated to be linked to peroxisomes (Tables 1 & 2), these data were focused on with interest. Not all peroxisome proteins were observed to change in abundance, as no significant changes in abundance were observed for Pxmp4 and Pex5 (Supp. Table 2). While at first the increase and decrease of peroxisomal proteins might seem contradictory, a review of their functions is revealing. For example, Baat is observed to be associated in higher amounts with LDs upon re-feeding which is consistent with the function of this enzyme in bile acid synthesis [59].

To validate some of the changes to the LD proteome we observed via LC-MS/MS, several candidate proteins were validated by Western blot analysis of purified LDs. In addition, to ensure the changes observed were due to an increase/decrease in LD-association and a change in global cellular protein abundance, these proteins were also investigated in whole liver homogenates. The proteins for these investigations were Plin5 and Acsl1. In both cases, the changes observed by LC-MS/MS analysis were mirrored by Western blot analysis; for instance, the quantified LC-MS/MS data for Acsl1 (Fig. 4) reveals a similar drop in abundance upon re-feeding as is observed by Western blotting (Fig. 7B).

Here we found that during the fasting state there is enrichment in Plin5 on LDs, along with an even greater increase in global Plin5 abundance in the liver (Fig. 7). Plin5 is mainly expressed in tissues with high levels of fatty acid oxidation, including the heart, liver, and skeletal muscle. It was recently demonstrated that Plin5 antagonizes lipase activities in the heart and is essential for maintaining LDs at detectable sizes [60]. In hepatocytes, Plin5 assists TG accumulation in LDs through a reduction of lipolysis and therefore release of fatty acids that could be substrates for β-oxidation [29]. Increased abundance of Plin5 on LDs during fasting (a catabolic state) is counterintuitive, given that Plin5 is inhibitory to lipolysis. The plausible explanation is that during fasting there is increased flux of adipose tissue-derived fatty acids to the liver with some being directly delivered to mitochondria for oxidation and the excess being stored in LDs. Plin5 could play a regulatory role of modulating lipolysis and hence prevent unregulated flux of fatty acids into mitochondria.

5. Conclusions

To our knowledge, this is the first comprehensive study describing the changes in the hepatic LD proteome in response to the physiological demands of fasting and re-feeding. Our analysis of the entire LD proteome adds to the growing understanding regarding the complexities of LD interactions with other cellular organelles. Analysis of LDs' compositional protein abundance has revealed that the major urinary proteins are highly abundant LD-associated proteins in hepatocytes that have been overlooked in previous studies. Additionally, our quantitative analysis revealed that the identified LD proteome is highly dynamic, with 161 proteins, nearly 20% of the observed 817 hepatic LD proteins, significantly varying in abundance during fasting and re-feeding. Immunoblotting validation of selected proteins also revealed that the LD proteome changes occur independent of global cellular protein abundance; large cellular changes in protein abundance observed for Plin2 and Plin5 were not reflected in the LD proteome, while Acsl1 was increased in LDs during fasting, even though its cellular abundance remained unchanged. We believe that the impact of this work is crucial for understanding the general hepatic physiology and particularly the complexity of LD metabolism. Our findings reveal the significance of well-controlled feeding in experimental design when investigating this cellular organelle.

Supplementary data to this article can be found online at https://doi.org/10.1016/j.jprot.2018.04.024.

Acknowledgments

This work was supported by grants from the Natural Sciences and Engineering Research Council of Canada (RGPIN-2017-04734) and the Canadian Institutes of Health Research to R.L. and a grant from the Natural Sciences and Engineering Research Council of Canada (RGPIN-2017-0579 to R.P.F. J.L. was a recipient of a postdoctoral fellowship from the Alberta Innovates-Health Solutions. A.D.Q. was a recipient of a postdoctoral fellowship from the Heart and Stroke Foundation of Canada during this study. D.A.K. was supported by studentships from Canadian Institutes for Heath Research (CIHR) and Alberta Innovates Technology Futures (AITF).

References

[1] R.V. Farese Jr., T.C. Walther, Lipid droplets finally get a little R-E-S-P-E-C-T, Cell 139 (5) (2009) 855–860.
[2] D.J. Murphy, The biogenesis and functions of lipid bodies in animals, plants and microorganisms, Prog. Lipid Res. 40 (5) (2001) 325–438.
[3] S.O. Olofsson, P. Bostrom, L. Andersson, M. Rutberg, J. Perman, J. Boren, Lipid droplets as dynamic organelles connecting storage and efflux of lipids, Biochim. Biophys. Acta 1791 (6) (2009) 448–458.
[4] N.L. Gluchowski, M. Becuwe, T.C. Walther, R.V. Farese Jr., Lipid droplets and liver disease: from basic biology to clinical implications, Nat. Rev. Gastroenterol. Hepatol. 14 (6) (2017) 343–355.
[5] T. Okumura, Role of lipid droplet proteins in liver steatosis, J. Physiol. Biochem. 67 (4) (2011) 629–636.
[6] S. Cermelli, Y. Guo, S.P. Gross, M.A. Welte, The lipid-droplet proteome reveals that droplets are a protein-storage depot, Curr. Biol. 16 (18) (2006) 1783–1795.
[7] A. Casanovas, R.R. Sprenger, K. Tarasov, D.E. Ruckerbauer, H.K. Hannibal-Bach, J. Zanghellini, O.N. Jensen, C.S. Ejsing, Quantitative analysis of proteome and lipidome dynamics reveals functional regulation of global lipid metabolism, Chem. Biol. 22 (3) (2015) 412–425.
[8] T. D'Aquila, D. Sirohi, J.M. Grabowski, V.E. Hedrick, L.N. Paul, A.S. Greenberg, R.J. Kuhn, K.K. Buhman, Characterization of the proteome of cytoplasmic lipid droplets in mouse enterocytes after a dietary fat challenge, PLoS One 10 (5) (2015) e0126823.
[9] S. Murphy, S. Martin, R.G. Parton, Lipid droplet-organelle interactions; sharing the fats, Biochim. Biophys. Acta 1791 (6) (2009) 441–447.
[10] Q. Gao, J.M. Goodman, The lipid droplet-a well-connected organelle, Front. Cell Dev. Biol. 3 (2015) 49.
[11] J.T. Haas, J. Miao, D. Chanda, Y. Wang, E. Zhao, M.E. Haas, M. Hirschey, B. Vaitheesvaran, R.V. Farese Jr., I.J. Kurland, M. Graham, R. Crooke, F. Foufelle, S.B. Biddinger, Hepatic insulin signaling is required for obesity-dependent expression of SREBP-1c mRNA but not for feeding-dependent expression, Cell Metab. 15 (6) (2012) 873–884.
[12] D.L. Brasaemle, N.E. Wolins, Isolation of lipid droplets from cells by density gradient centrifugation, Curr Protoc Cell Biol Chapter 3, Unitas 3 (2006) 15.
[13] H. Wang, A.D. Quiroga, R. Lehner, Analysis of lipid droplets in hepatocytes, Methods Cell Biol. 116 (2013) 107–127.
[14] B. Alsaikhan, R. Fahlman, J. Ding, E. Tredget, P.D. Metcalfe, Proteomic profile of an acute partial bladder outlet obstruction, Can. Urol. Assoc. J. 9 (3–4) (2015) E114–21.
[15] D.A. Kramer, M.A. Eldeeb, M. Wuest, J. Mercer, R.P. Fahlman, Proteomic characterization of EL4 lymphoma derived tumors upon chemotherapy treatment reveals potential roles for lysosomes and caspase-6 during tumor cell death in vivo, Proteomics 17 (2017) 1700060.
[16] J.A. Vizcaino, A. Csordas, N. del-Toro, J.A. Dianes, J. Griss, I. Lavidas, G. Mayer, Y. Perez-Riverol, F. Reisinger, T. Ternent, Q.W. Xu, R. Wang, H. Hermjakob, 2016 update of the PRIDE database and its related tools, Nucleic Acids Res. 44 (D1) (2016) D447–56.
[17] E. Ahrne, L. Molzahn, T. Glatter, A. Schmidt, Critical assessment of proteome-wide label-free absolute abundance estimation strategies, Proteomics 13 (17) (2013) 2567–2578.
[18] H. Wang, D. Gilham, R. Lehner, Proteomic and lipid characterization of apolipoprotein B-free luminal lipid droplets from mouse liver microsomes: implications for very low density lipoprotein assembly, J. Biol. Chem. 282 (45) (2007) 33218–33226.
[19] Z. Cui, J.E. Vance, M.H. Chen, D.R. Voelker, D.E. Vance, Cloning and expression of a novel phosphatidylethanolamine N-methyltransferase. A specific biochemical and cytological marker for a unique membrane fraction in rat liver, J. Biol. Chem. 268 (22) (1993) 16655–16663.
[20] H. Wang, E. Wei, A.D. Quiroga, X. Sun, N. Touret, R. Lehner, Altered lipid droplet dynamics in hepatocytes lacking triacylglycerol hydrolase expression, Mol. Biol. Cell 21 (12) (2010) 1991–2000.
[21] S.A. Khan, E.E. Wollaston-Hayden, T.W. Markowski, L. Higgins, D.G. Mashek, Quantitative analysis of the murine lipid droplet-associated proteome during diet-induced hepatic steatosis, J. Lipid Res. 56 (12) (2015) 2260–2272.

[22] A.E. Crunk, J. Monks, A. Murakami, M. Jackman, P.S. Maclean, M. Ladinsky, E.S. Bales, S. Cain, D.J. Orlicky, J.L. McManaman, Dynamic regulation of hepatic lipid droplet properties by diet, PLoS One 8 (7) (2013) e67631.
[23] H. Mi, X. Huang, A. Muruganujan, H. Tang, C. Mills, D. Kang, P.D. Thomas, PANTHER version 11: expanded annotation data from Gene Ontology and Reactome pathways, and data analysis tool enhancements, Nucleic Acids Res. 45 (D1) (2017) D183–D189.
[24] P. Shannon, A. Markiel, O. Ozier, N.S. Baliga, J.T. Wang, D. Ramage, N. Amin, B. Schwikowski, T. Ideker, Cytoscape: a software environment for integrated models of biomolecular interaction networks, Genome Res. 13 (11) (2003) 2498–2504.
[25] G. Bindea, J. Galon, B. Mlecnik, CluePedia Cytoscape plugin: pathway insights using integrated experimental and in silico data, Bioinformatics 29 (5) (2013) 661–663.
[26] D. Szklarczyk, J.H. Morris, H. Cook, M. Kuhn, S. Wyder, M. Simonovic, A. Santos, N.T. Doncheva, A. Roth, P. Bork, L.J. Jensen, C. von Mering, The STRING database in 2017: quality-controlled protein-protein association networks, made broadly accessible, Nucleic Acids Res. 45 (D1) (2017) D362–D368.
[27] J.M. Ellis, S.M. Mentock, M.A. Depetrillo, T.R. Koves, S. Sen, S.M. Watkins, D.M. Muoio, G.W. Cline, H. Taegtmeyer, G.I. Shulman, M.S. Willis, R.A. Coleman, Mouse cardiac acyl coenzyme a synthetase 1 deficiency impairs fatty acid oxidation and induces cardiac hypertrophy, Mol. Cell. Biol. 31 (6) (2011) 1252–1262.
[28] J.M. Ellis, L.O. Li, P.C. Wu, T.R. Koves, O. Ilkayeva, R.D. Stevens, S.M. Watkins, D.M. Muoio, R.A. Coleman, Adipose acyl-CoA synthetase-1 directs fatty acids toward beta-oxidation and is required for cold thermogenesis, Cell Metab. 12 (1) (2010) 53–64.
[29] H. Li, Y. Song, L.J. Zhang, Y. Gu, F.F. Li, S.Y. Pan, L.N. Jiang, F. Liu, J. Ye, Q. Li, LSDP5 enhances triglyceride storage in hepatocytes by influencing lipolysis and fatty acid beta-oxidation of lipid droplets, PLoS One 7 (6) (2012) e36712.
[30] M. Conte, C. Franceschi, M. Sandri, S. Salvioli, Perilipin 2 and age-related metabolic diseases: a new perspective, Trends Endocrinol. Metab. 27 (12) (2016) 893–903.
[31] H. Zhang, Y. Wang, J. Li, J. Yu, J. Pu, L. Li, S. Zhang, G. Peng, F. Yang, P. Liu, Proteome of skeletal muscle lipid droplet reveals association with mitochondria and apolipoprotein a-I, J. Proteome Res. 10 (10) (2011) 4757–4768.
[32] H.L. Ploegh, A lipid-based model for the creation of an escape hatch from the endoplasmic reticulum, Nature 448 (7152) (2007) 435–438.
[33] S. Mishra, R. Khaddaj, S. Cottier, V. Stradalova, C. Jacob, R. Schneiter, Mature lipid droplets are accessible to ER luminal proteins, J. Cell Sci. 129 (20) (2016) 3803–3815.
[34] V.W. Dolinsky, D. Gilham, M. Alam, D.E. Vance, R. Lehner, Triacylglycerol hydrolase: role in intracellular lipid metabolism, Cell. Mol. Life Sci. 61 (13) (2004) 1633–1651.
[35] D. Gilham, M. Alam, W. Gao, D.E. Vance, R. Lehner, Triacylglycerol hydrolase is localized to the endoplasmic reticulum by an unusual retrieval sequence where it participates in VLDL assembly without utilizing VLDL lipids as substrates, Mol. Biol. Cell 16 (2) (2005) 984–996.
[36] K.W. Ko, B. Erickson, R. Lehner, Es-x/Ces1 prevents triacylglycerol accumulation in McArdle-RH7777 hepatocytes, Biochim. Biophys. Acta 1791 (12) (2009) 1133–1143.
[37] A.D. Quiroga, L. Li, M. Trotzmuller, R. Nelson, S.D. Proctor, H. Kofeler, R. Lehner, Deficiency of carboxylesterase 1/esterase-x results in obesity, hepatic steatosis, and hyperlipidemia, Hepatology 56 (6) (2012) 2188–2198.
[38] D. Binns, T. Januszewski, Y. Chen, J. Hill, V.S. Markin, Y. Zhao, C. Gilpin, K.D. Chapman, R.G. Anderson, J.M. Goodman, An intimate collaboration between peroxisomes and lipid bodies, J. Cell Biol. 173 (5) (2006) 719–731.
[39] I.J. Lodhi, C.F. Semenkovich, Peroxisomes: a nexus for lipid metabolism and cellular signaling, Cell Metab. 19 (3) (2014) 380–392.
[40] M. Beller, D. Riedel, L. Jansch, G. Dieterich, J. Wehland, H. Jackle, R.P. Kuhnlein, Characterization of the Drosophila lipid droplet subproteome, Mol. Cell. Proteomics 5 (6) (2006) 1082–1094.
[41] H.C. Wan, R.C. Melo, Z. Jin, A.M. Dvorak, P.F. Weller, Roles and origins of leukocyte lipid bodies: proteomic and ultrastructural studies, FASEB J. 21 (1) (2007) 167–178.
[42] Y. Ohsaki, M. Suzuki, T. Fujimoto, Open questions in lipid droplet biology, Chem. Biol. 21 (1) (2014) 86–96.
[43] M. Liu, R. Ge, W. Liu, Q. Liu, X. Xia, M. Lai, L. Liang, C. Li, L. Song, B. Zhen, J. Qin, C. Ding, Differential proteomics profiling identifies LDPs and biological functions in high-fat diet-induced fatty livers, J. Lipid Res. 58 (4) (2017) 681–694.
[44] C. Baumeier, D. Kaiser, J. Heeren, L. Scheja, C. John, C. Weise, M. Eravci, M. Lagerpusch, G. Schulze, H.G. Joost, R.W. Schwenk, A. Schurmann, Caloric restriction and intermittent fasting alter hepatic lipid droplet proteome and diacylglycerol species and prevent diabetes in NZO mice, Biochim. Biophys. Acta 1851 (5) (2015) 566–576.
[45] D.L. Brasaemle, G. Dolios, L. Shapiro, R. Wang, Proteomic analysis of proteins associated with lipid droplets of basal and lipolytically stimulated 3T3-L1 adipocytes, J. Biol. Chem. 279 (45) (2004) 46835–46842.
[46] Y. Fujimoto, H. Itabe, J. Sakai, M. Makita, J. Noda, M. Mori, Y. Higashi, S. Kojima, T. Takano, Identification of major proteins in the lipid droplet-enriched fraction isolated from the human hepatocyte cell line HuH7, Biochim. Biophys. Acta 1644 (1) (2004) 47–59.
[47] R. Bartz, W.H. Li, B. Venables, J.K. Zehmer, M.R. Roth, R. Welti, R.G. Anderson, P. Liu, K.D. Chapman, Lipidomics reveals that adiposomes store ether lipids and mediate phospholipid traffic, J. Lipid Res. 48 (4) (2007) 837–847.
[48] P. Liu, R. Bartz, J.K. Zehmer, Y.S. Ying, M. Zhu, G. Serrero, R.G. Anderson, Rab-regulated interaction of early endosomes with lipid droplets, Biochim. Biophys. Acta 1773 (6) (2007) 784–793.
[49] S. Martin, K. Driessen, S.J. Nixon, M. Zerial, R.G. Parton, Regulated localization of Rab18 to lipid droplets: effects of lipolytic stimulation and inhibition of lipid droplet catabolism, J. Biol. Chem. 280 (51) (2005) 42325–42335.
[50] S. Turro, M. Ingelmo-Torres, J.M. Estanyol, F. Tebar, M.A. Fernandez, C.V. Albor, K. Gaus, T. Grewal, C. Enrich, A. Pol, Identification and characterization of associated with lipid droplet protein 1: a novel membrane-associated protein that resides on hepatic lipid droplets, Traffic 7 (9) (2006) 1254–1269.
[51] Y. Ohsaki, J. Cheng, M. Suzuki, Y. Shinohara, A. Fujita, T. Fujimoto, Biogenesis of cytoplasmic lipid droplets: from the lipid ester globule in the membrane to the visible structure, Biochim. Biophys. Acta 1791 (6) (2009) 399–407.
[52] S. Ozeki, J. Cheng, K. Tauchi-Sato, N. Hatano, H. Taniguchi, T. Fujimoto, Rab18 localizes to lipid droplets and induces their close apposition to the endoplasmic reticulum-derived membrane, J. Cell Sci. 118 (Pt 12) (2005) 2601–2611.
[53] P. Liu, Y. Ying, Y. Zhao, D.I. Mundy, M. Zhu, R.G. Anderson, Chinese hamster ovary K2 cell lipid droplets appear to be metabolic organelles involved in membrane traffic, J. Biol. Chem. 279 (5) (2004) 3787–3792.
[54] S. Murphy, S. Martin, R.G. Parton, Lipid droplet-organelle interactions; sharing the fats, Biochim. Biophys. Acta 1791 (6) (2009) 441–447.
[55] J. Bouchoux, F. Beilstein, T. Pauquai, I.C. Guerrera, D. Chateau, N. Ly, M. Alqub, C. Klein, J. Chambaz, M. Rousset, J.M. Lacorte, E. Morel, S. Demignot, The proteome of cytosolic lipid droplets isolated from differentiated Caco-2/TC7 enterocytes reveals cell-specific characteristics, Biol. Cell. 103 (11) (2011) 499–517.
[56] Y. Zhou, L. Rui, Major urinary protein regulation of chemical communication and nutrient metabolism, Vitam. Horm. 83 (2010) 151–163.
[57] K. Athenstaedt, D. Zweytick, A. Jandrositz, S.D. Kohlwein, G. Daum, Identification and characterization of major lipid particle proteins of the yeast Saccharomyces cerevisiae, J. Bacteriol. 181 (20) (1999) 6441–6448.
[58] W. Wang, S. Wei, L. Li, X. Su, C. Du, F. Li, B. Geng, P. Liu, G. Xu, Proteomic analysis of murine testes lipid droplets, Sci. Rep. 5 (2015) 12070.
[59] S. Ferdinandusse, S. Denis, P.L. Faust, R.J. Wanders, Bile acids: the role of peroxisomes, J. Lipid Res. 50 (11) (2009) 2139–2147.
[60] K. Kuramoto, T. Okamura, T. Yamaguchi, T.Y. Nakamura, S. Wakabayashi, H. Morinaga, M. Nomura, T. Yanase, K. Otsu, N. Usuda, S. Matsumura, K. Inoue, T. Fushiki, Y. Kojima, T. Hashimoto, F. Sakai, F. Hirose, T. Osumi, Perilipin 5, a lipid droplet-binding protein, protects heart from oxidative burden by sequestering fatty acid from excessive oxidation, J. Biol. Chem. 287 (28) (2012) 23852–23863.